IJAME
Int. J. of Applied Mechanics and Engineering, 2024, vol.29, No.3, pp.82-100
DOI: 10.59441/ijame/190397

START-OFF MHD ELECTROKINETIC COUETTE FLOW IN AN ANNULUS: A RIEMANN-SUM APPROXIMATION APPROACH

Michael O. Oni*
Department of Mathematics, Ahmadu Bello University, Zaria, NIGERIA
E-mail: michaeloni29@yahoo.com

Basant K. Jha
Department of Mathematics, Ahmadu Bello University, NIGERIA

Junaid M. Abba
Department of Mathematics, Ahmadu Bello University, Zaria, NIGERIA

Baba I. Mundi
ICT, Nigerian Institute of Transport Technology, NIGERIA

Olaife H Adebayo
Department of Mathematics, Ahmadu Bello University, Zaria, NIGERIA

The time dependent Couette flow (CF) of a conducting fluid formed between two concentric tubes with variable electric potential and accelerated motion of the outer cylinder is investigated. The governing electric field potential as well as the momentum equivalences are gotten from Poisson-Boltzmann and Navier Stokes Eqs respectively. As a promising tool for solving time-dependent problems, the Laplace-transform technique is employed to get analytical solution for electric field and velocity profile in Laplace realm. By employing the Riemann sum approximation (RSA) simulation, the results are obtained numerically in time-domain. During the graphical and numerical simulation of obtained results, it is found that the magnitude of electrokinetic effect as well as Debye-Hückel parameter play important role in flow formation and mass flow rate in the horizontal annulus. Further, velocity, mass flow rate, and skin-friction decrease with increase in Debye-Hückel parameter at all-time regardless of the mode of application of magnetic field. In addition, mass flowrate can be enhanced with increasing Hartmann number when the magnetic-field is fixed relative to the moving cylinder.

Key words: electrokinetic; unsteady; Couette flow; annuli; MHD.

1. Introduction

Electrokinetics refer to the study of electrically driven mechanical motion of charged particles or fluid. This phenomenon was first observed by Reuss in 1808, in the electrophoresis of clay particles [1]. This study continues to gain attention owing to its applications in water supply, medical science and electro-mechanical devices. One of the most significant application is the design of micropumping devices used in drug delivery, fuel supply and biochemical reactive platform [2]. Generally, an electric double-layer (EDL) is induced when solid surfaces which usually acquire a negative electric charge comes in contact with a fluid containing dissociated salt [3, 4]. This interaction generates an electric force near the wall, thereby provoking fluid motion, which subsequently transmitted to the bulk fluid by viscous forces [5].

* To whom correspondence should be addressed

It is well-known that the basic factors controlling the flow-rate in electroosmotic pumping are: the strength of the externally applied electric field, the cross-sectional dimensions of the annulus, the microchannel surface charge density and the ion density/PH of the working fluid [6]. Although increasing the magnitude of externally applied electric field enhances flow-rate, but this can cause a huge increase in the temperature of the fluid and as a result increasing the Joule heating effect, which is not advantageous [4]. Therefore, other mechanism must be used to achieve high volume flow rate. A lot of efforts and researches both theoretically and experimentally have been conducted to solve the aforementioned problem [7-13]. Most of which have used pulsating force as a control mechanism for flow-rate.

The study of magnetohydrodynamics in annular geometry has rapidly become a research field due to its technological applications, such as drilling operation of oil and gas wells. By assuming that the magnetic lines of forces are fixed relative to the fluid, Katagiri [14] investigated the Couette flow formation of viscous, incompressible and electrically conducting fluid between two-infinite parallel plane walls subjected to transversely applied magnetic field and found that skin-friction increases with increase in Hartmann number. Later, Muhuri [15] extended the problem by imposing a uniform suction velocity on the walls and obtained that skin-friction is enhanced by increasing suction parameter. Singh and Kumar [16] on the other hand considered the same problem by assuming that the magnetic lines of force are fixed relative to the moving plate for both the impulsive and accelerated motion of the moving plates and concluded that the effect of magnetic field is to increase fluid velocity for both cases.

In annular geometry, the study of electrically conducting fluid was first carried out by Globe [17]. Since then, different articles have been credited to capture a more physical phenomena [18-22]. Jha and Apere [22], investigated the unsteady MHD Couette flow in an annuli by using the Riemann-sum approximation technique to obtain the results from Laplace domain to time domain. They deduced that skin-friction is a decreasing function of Hartmann number at the outer surface of the inner cylinder. Also, they did not analyse the role of magnetic field as well as accelerated motion of the boundary on volumetric flow-rate. Other recent related articles on electroosmotic flow and magnetic field can be seen in [23, 24].

The novelty of the current work is the development of mathematical models to theoretically analyse the unsteady electrokinetic Couette flow in a horizontal annulus filled with electrically conducting fluid. One real-world application of this configuration can be found in the design and optimization of certain types of electromagnetic pumps. These pumps utilize the principles of MHD to move electrically conducting fluids, such as liquid metals or molten salts, without the need for any moving mechanical parts. Another physical application of start-up flow can be seen during the ignition of a rocket engine, the start-up flow plays a vital role in establishing the necessary conditions for efficient combustion and thrust generation. This entire article can be viewed as an extension of [22] by incorporating the electrokinetic effect due to its applications in micropumping devices. Further, we intend to investigate the role of magnetic field in transverse direction as well as accelerated motion of the cylinder surface on volumetric flow-rate and skin-friction, so as to serve as a control mechanism. The governing Eqs as well as the analytical solutions are presented in section two while the discussion of results and conclusions respectively follow in subsequent sections.

2. Mathematical construction

A time dependent, fully developed, laminar flow of conducting fluid between two concentric tubes with variable electric potential is considered. The radiuses of the inside and outside cylinders are assumed to be r_1 and r_2 respectively. The inner cylinder is assumed fixed outside while the outer tube is assumed to be augmented with a velocity comparative to η^m, where η is time and m is a positive integer. The flow is driven by combined external voltage gradient and accelerated motion of the outer cylinder. Electric potential ζ_1, ζ_2 such that $\zeta_2 > \zeta_1$ are applied on the surface of the inner tube and outer cylinder respectively (see Fig.1). The EDL follows Boltzmann distribution, so that the convection due to ion effects are insignificant. Also, the wall potentials are assumed small, so that Debye-Huckel linearization to be useable. All other physical thermodynamics parameters are assumed constant.

Electric field potential

Following assumptions above, the electrical potential is obtained as:

$$\nabla^2\phi = -\frac{\rho_e}{\varepsilon}. \tag{2.1}$$

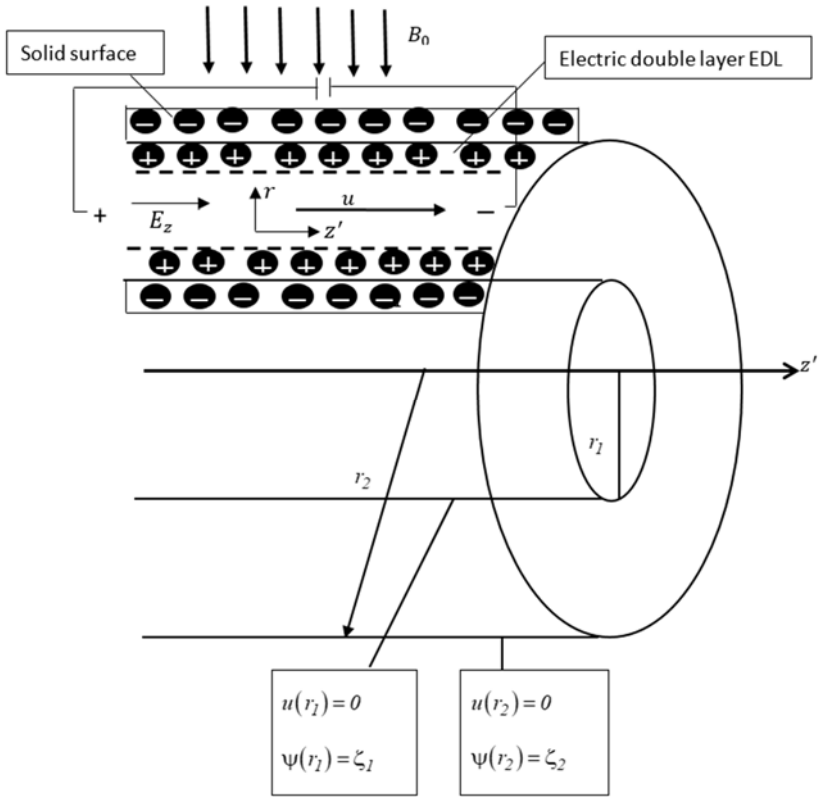

Fig.1. Schematic diagram of the problem.

The potential, ϕ is due to combination of externally forced field Φ and EDL potential ψ'. Where ρ_e is the net volume charge density of symmetric electrolyte and defined as [3]:

$$\rho_e = -2FzC_0 \sinh\left(\frac{zF\psi'}{R'T}\right), \qquad \nabla = \frac{\partial}{\partial r}\vec{i} + \frac{1}{r}\frac{\partial}{\partial\phi}\vec{j} + \frac{\partial}{\partial z'}\vec{k}. \tag{2.2}$$

For fully developed flow, the external potential gradient is in the axial direction only $\phi = \phi(r)$ and $\psi' = \psi'(r)$:

$$\left[\frac{1}{r}\frac{\partial}{\partial r}\left(r\frac{\partial\psi'}{\partial r}\right)\right] = \frac{2FzC_0}{\varepsilon}\sinh\left(\frac{zF\psi'}{R'T}\right), \tag{2.3}$$

subject to the boundary condition:

$$\psi'(r_1) = \zeta_1, \qquad \psi'(r_2) = \zeta_2 \tag{2.4}$$

where ζ_1, ζ_2 are zeta-potential at the surfaces of the cylinders.

Since the wall potential are assumed low enough for Debye-Huckel linearization to be valid, Eqs (2.3) and (2.4) in dimensionless form become [12]:

$$\frac{d^2\psi}{dR^2}+\frac{1}{R}\frac{d\psi}{dR}-\kappa^2\psi=0\,, \tag{2.5}$$

$$\psi(1)=\zeta_r\,,\qquad \psi(\lambda)=1\,. \tag{2.6}$$

Velocity profile

The momentum equation governing the flow formation of an electrically conducting fluid in a horizontal concentric cylinder is obtained from the Navier-Stokes equation in vectorial form as [20]:

$$\rho_f\left(\frac{\partial v}{\partial t}+(v\cdot\nabla)v\right)=-\nabla p+\mu\nabla^2 v+\rho_e E_{z'}+JXB\,. \tag{2.7}$$

Considering a time dependent magnetohydrodynamically fully developed flow in a concentric annulus, the above equation reduces to:

$$\frac{\partial u}{\partial \eta}=\nu\left(\frac{\partial^2 u}{\partial r^2}+\frac{1}{r}\frac{\partial u}{\partial r}\right)-\frac{\sigma B_0^2}{\rho}\left[u-Ku'\eta^m\right]+\varepsilon\left(\frac{d^2\psi'}{dr^2}+\frac{1}{r}\frac{d\psi'}{dr}\right)E_{z'}, \tag{2.8}$$

subject to the following initial and boundary conditions:

$$u(r,0)=0\,,\qquad u(r_1,\eta)=0\,,\qquad u(r_2,\eta)=u'\eta^{m'} \tag{2.9}$$

where m' is a positive integer (in this current article, we have taken $m'=1$ which corresponds to the accelerated motion case), K is a constant which assumes value zero or one, is such that:

$$K=\begin{cases}0 & \text{when } B_0 \text{ is fixed relative to the fluid,}\\ 1 & \text{when } B_0 \text{ is fixed relative to the moving cylinder.}\end{cases} \tag{2.10}$$

Using the following dimensionless parameters on Eqs (2.8) and (2.9), we have [3, 4, 22]:

$$\begin{gathered}R=\frac{r}{r_1}\,,\quad U=\frac{u\nu}{u'r_1^2}\,,\quad M^2=\frac{\sigma B_0^2 r_1^2}{\nu\rho}\,,\quad t=\frac{\eta\nu}{r_1^2}\,,\quad \lambda=\frac{r_2}{r_1}\,,\quad \zeta_r=\frac{\zeta_1}{\zeta_2}\,,\\ \psi=\frac{zF\psi'}{R'T}\,,\quad \kappa=\frac{r_1}{\lambda_D}\,,\quad \lambda_D=\left[\frac{\varepsilon R'T}{2F^2Z^2C_0}\right]^{1/2}\,,\quad G=\frac{2F^2Z^2C_0r_1^2}{R'Tu'}E_{z'}\,.\end{gathered} \tag{2.11}$$

$$\frac{\partial U}{\partial t}=\left(\frac{\partial^2 U}{\partial R^2}+\frac{1}{R}\frac{\partial U}{\partial R}\right)-M^2\left[U-Kt\right]+G\psi, \tag{2.12}$$

subject to:

$$U(R,0)=0, \quad U(1,t)=0, \quad U(\lambda,t)=t. \tag{2.13}$$

Mathematical solution of the problem

It is important to note that the electric potential equation is obtained from the Poison equation and therefore only the steady state solution is possible. Hence the solution of (2.5 and 2.6) is obtained as:

$$\psi(R)=C_1 I_0(\kappa R)+C_2 K_0(\kappa R), \tag{2.14}$$

where I_0, K_0 are Bessel's functions and C_1 and C_2 are constants defined by:

$$C_1=\frac{K_0(\kappa)-\zeta_r K_0(\kappa\lambda)}{I_0(\kappa\lambda)K_0(\kappa)-I_0(\kappa)K_0(\kappa\lambda)}, \quad C_2=\frac{\zeta_r I_0(\kappa\lambda)-I_0(\kappa)}{I_0(\kappa\lambda)K_0(\kappa)-I_0(\kappa)K_0(\kappa\lambda)}. \tag{2.15}$$

Using the Laplace transform (*LT)* approach, analytical solution of Eq.(2.12) with condition (2.13) can be obtained:

$$L\left[U(Y,t)\right]=\bar{U}(Y,S)=\int_0^\infty U(Y,t)\exp(-St)\,dt, \quad S>0, \tag{2.16}$$

Applying the Laplace transformation of Eq.(2.16) on Eqs (2.12) and (2.13), we obtained:

$$\frac{d^2\bar{U}}{dR^2}+\frac{1}{R}\frac{d\bar{U}}{dR}-\bar{U}\left[M^2-S\right]=-\frac{M^2K}{S^2}-\frac{G\left[C_1 I_0(\kappa R)+C_2 K_0(\kappa R)\right]}{S}. \tag{2.17}$$

Subject to:

$$\bar{U}(1,S)=0, \quad \bar{U}(\lambda,S)=\frac{1}{S^2}. \tag{2.18}$$

Equation (2.17) with conditions (2.18) are solved to obtain fluid velocity in terms of modified Bessel's function as:

$$\bar{U}(R,S)=C_3 I_0(\delta R)+C_4 K_0(\delta R)+\frac{M^2K}{S^2\left(S+M^2\right)}+\frac{G\left[C_1 I_0(\kappa R)+C_2 K_0(\kappa R)\right]}{S\left(S+M^2-\kappa^2\right)} \tag{2.19}$$

where: $C_3=\dfrac{D_1}{K_0(\delta\lambda)I_0(\delta)-K_0(\delta)I_0(\delta\lambda)}, \quad C_4=\dfrac{D_2}{K_0(\delta\lambda)I_0(\delta)-K_0(\delta)I_0(\delta\lambda)},$

$$D_1=\frac{G\left[K_0(\delta)-\zeta_r K_0(\lambda\delta)\right]}{S\left(S+M^2-\kappa^2\right)}+\frac{M^2K\left[K_0(\delta)-\zeta_r K_0(\lambda\delta)\right]}{S\left(S+M^2\right)}-\frac{K_0(\delta)}{S^2}, \tag{2.20}$$

$$D_2=\frac{I_0(\delta)}{S^2}+\frac{G\left[\zeta_r I_0(\lambda\delta)-I_0(\delta)\right]}{S\left(S+M^2-\kappa^2\right)}+\frac{M^2K\left[I_0(\lambda\delta)-I_0(\delta)\right]}{S\left(S+M^2\right)}, \quad \delta=\sqrt{S+M^2}.$$

The transient skin frictions at the outer and inner tunes are respectively obtained as follow:

$$\bar{\tau} = \left.\frac{d\bar{U}(R,S)}{dR}\right|_{R=1} = \delta\left[C_3 I_1(\delta) - C_4 K_1(\delta)\right] + \frac{G_2\kappa\left[C_1 I_1(\kappa) - C_2 K_1(\kappa)\right]}{S\left(S + M^2 - \kappa^2\right)}, \tag{2.21}$$

$$\bar{\tau} = \left.\frac{d\bar{U}(R,S)}{dR}\right|_{R=\lambda} = \delta\left[C_3 I_1(\lambda\delta) - C_4 K_1(\lambda\delta)\right] + \frac{G\kappa\left[C_1 I_1(\lambda\kappa) - C_2 K_1(\lambda\kappa)\right]}{S\left(S + M^2 - \kappa^2\right)}. \tag{2.22}$$

Also, the dimensionless transient mass flux is given by:

$$\begin{aligned}\bar{Q} = \int_1^{\lambda} RU(R)\,dR = \frac{C_3}{\delta}\left[\lambda I_1(\lambda\delta) - I_1(\delta)\right] - \frac{C_4}{\delta}\left[\lambda K_1(\lambda\delta) - K_1(\delta)\right] + \frac{\left(\lambda^2 - 1\right)M^2 K}{2S^2\left(M^2 + S\right)} + \\ + \frac{G}{S\left(S + M^2 - \kappa^2\right)\kappa}\left[\frac{C_1}{\kappa}\left[\lambda I_1(\lambda\kappa) - I_1(\kappa)\right] - \frac{C_2}{\kappa}\left[\lambda K_1(\lambda\kappa) - K_1(\kappa)\right]\right].\end{aligned} \tag{2.23}$$

The solutions obtained for flow formation from Eqs (2.19)-(2.23) are in Laplace domain. Due to the complexity of the solutions, we employed the Riemann-sum approximation technique [27-29] to transform from Laplace domain to time domain. In this technique, functions in the Laplace domain, $\bar{U}(R,S)$ can be reversed to time realm by single summation:

$$U(R,t) = \frac{e^{\varepsilon' t}}{t}\left[\frac{1}{2}\bar{U}(R,\varepsilon') + Re\sum_{n=1}^{m}\bar{U}\left(R,\varepsilon' + \frac{in\pi}{t}\right)(-1)^n\right], \quad 1 \le R \le \lambda \tag{2.24}$$

where Re denotes to the real part of $i = \sqrt{-1}$, m is the number of terms used in the RSA and ε is the real part of the Bromwich contour. The RSA for the inversion involves a single summation for the numerical process. Its correctness depends on the value of ε' and the error led by m. According to Tzou [28], the value of εt that best satisfied the result is 4.7.

3. Results and discussion

This work is dedicated to investigate the effect of electric potential and applied magnetic field on Couette flow formation of a conducting fluid in a horizontal annulus. Before establishing the role of various governing parameters, it is expedient to first check the accuracy of the solution obtained by comparing with published article in literature in the absence of externally applied electric field. Table 1 presents a numerical comparison between the present work velocity with those of Jha and Apere [22] in the absence of electrokinetic effect $(G = 0)$. From this numerical computation, an excellent agreement is found. Table 2 on the other hand presents percentage change due to application of electrokinetic effect. It is found that percentage change due to electrokinetic effect are pronouncedly felt around the center of the annulus.

To evaluate the role of governing parameters such as Debye-Hückel parameter (κ), Hartmann number (M), annular gap (λ), magnitude of electric potential (G) and dimensional time (t), we typically used the values of the physical parameters that have been utilized in previously published work in electroosomotic flows [26]. For computational purpose, in this research, $0 \le \kappa \le 30$ to analyse the physical situations ranging from thin to huge EDL, the zeta potentials at the walls are assumed over $0 \le \zeta_r \le 1$, and $0 \le M \le 5$ for Hartmann number.

Table 1. Comparison of velocity profile obtained versus those obtained by Jha and Apere [22] for $M = 2.0, t = 5.0, \lambda = 2.0$.

	$K = 0$		$K = 0$	
R	Jha and Apere [22]	Present work $(G = 0)$	Jha and Apere [22]	Present work $(G = 0)$
1.0	*0.0000*	*0.0000*	*0.0000*	*0.0000*
1.2	*0.7230*	*0.7230*	*1.9539*	*1.9539*
1.4	*1.4484*	*1.4484*	*3.1635*	*3.1635*
1.6	*2.3077*	*2.3077*	*3.9571*	*3.9571*
1.8	*3.4363*	*3.4363*	*4.5281*	*4.5281*
2.0	*5.0001*	*5.0001*	*5.0001*	*5.0001*

Table 2. Percentage change in flow formation due to EDL for $M = 2.0, t = 5.0, \lambda = 2.0, \kappa = 0.1, \zeta_r = 1.0$.

	$G = 0$		$G = 1$			
R	$K = 0$	$K = 1$	$K = 0$	$K = 1$	$K = 0$ (% change)	$K = 1$ (% change)
1.0	*0.0000*	*0.0000*	*0.0000*	*0.0000*	*0.00*	*0.00*
1.2	*0.7230*	*0.7230*	*0.7854*	*2.0163*	*8.63*	*3.19*
1.4	*1.4484*	*1.4484*	*1.5354*	*3.2505*	*5.99*	*2.75*
1.6	*2.3077*	*2.3077*	*2.3913*	*4.0407*	*3.62*	*2.12*
1.8	*3.4363*	*3.4363*	*3.4916*	*4.5834*	*1.61*	*1.22*
2.0	*5.0001*	*5.0001*	*5.0001*	*5.0001*	*0.00*	*0.00*

Electric potential

Figure 2 depicts the dimensionless electrostatic potential in the annulus as a role of ζ. The EDL potential is found to be higher at the walls owing to the applied external voltage at the surfaces of the cylinders.

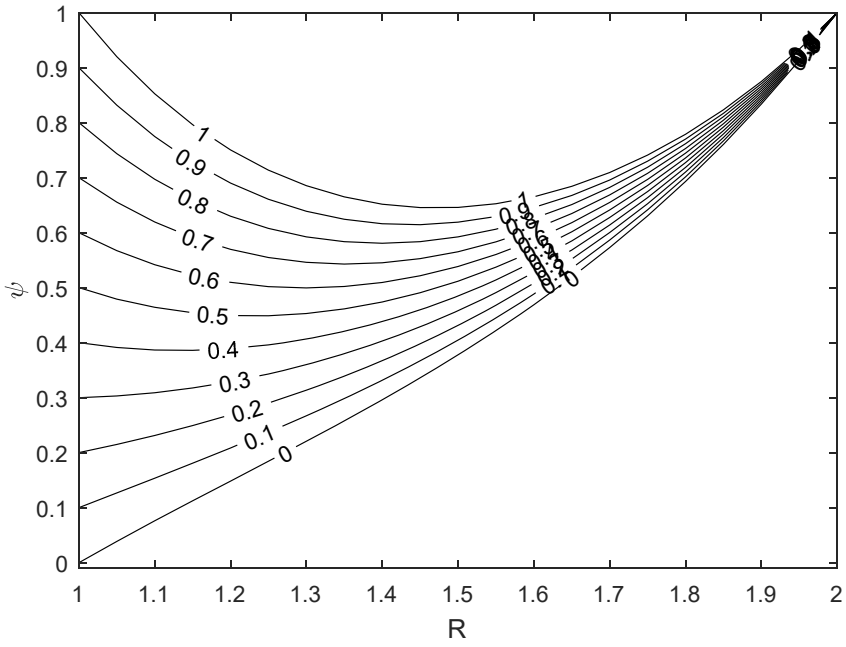

Fig.2. Electric potential for different values of ζ_r at $\lambda = 2.0$, $\kappa = 3.0$.

Also, as the zeta potential at the outer surfaces of inner cylinder leaves asymmetric state, $(\zeta_r \neq 0)$, the electric potential in the annulus gradually changes form a linear function to a parabolic function. This scenario can be attributed to the zeta-potential supplied at the surfaces of the cylinders. Furthermore, the least electric potential is felt towards the centre of the annulus for the case of symmetric wall zeta potential.

Velocity profile

This sub-section is devoted to presentation of velocity profile results for the current problem. The figure captions with (a) signifies that magnetic field is fixed relative to fluid $(K=0)$ and caption (b) indicates when magnetic field is fixed relative to moving cylinder $(K=1)$.

Figures 3a and 3b examine the impact of dimensionless time (t) and Debye-Hückel parameter (κ) on velocity profile in the annulus for the cases when magnetic field is fixed relative to fluid and moving cylinder respectively. Fluid motion is improved by dimensionless time but retarded with increase in κ throughout the annulus. This is because increasing κ, decreases the EDL length and therefore reduces the externally applied voltage gradient which should have increased the kinetic energy and hence leading to decrease in fluid velocity in the annulus. Conversely, due to the accelerated motion of the outer cylinder, a nonstop increase in velocity is inevitable.

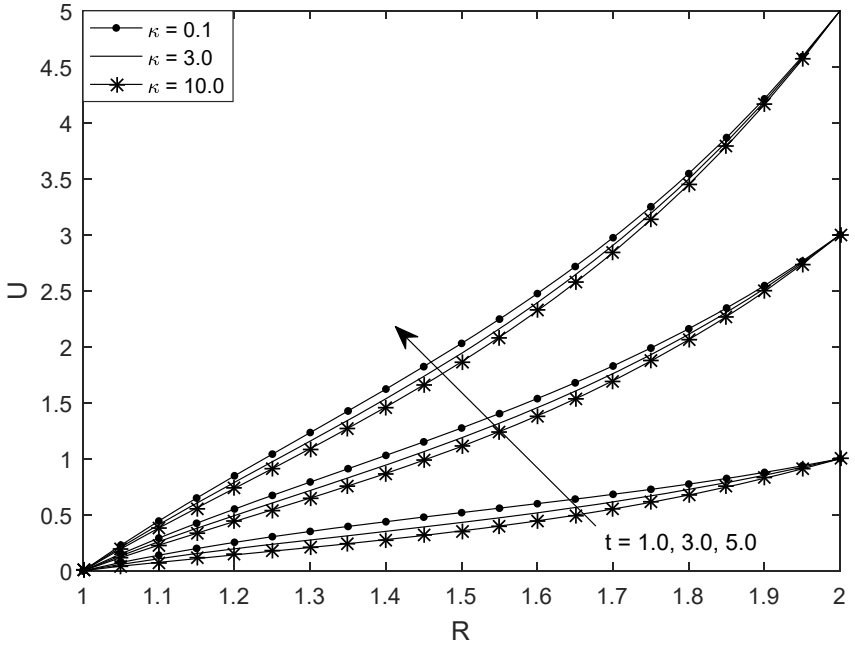

Fig.3a. Velocity profile for different values of κ at different time t for $M=2.0$, $\lambda=2.0$, $G=2.0$, $\zeta_r=1.0$, $K=0$.

Figures 4a and 4b illustrate fluid velocity as a function of Hartmann number (M) and magnitude of electric potential (G) for $K=0$ and $K=1$ respectively in the horizontal annulus filled with electrically conducting fluid. It is obvious from these graphs that velocity increase as G increases regardless of the mode of application of the magnetic field. This is credited to the point that rise in magnitude of EDL rises with the electric potential and therefore enhancing fluid motion. Then again, velocity declines with growth in M when $K=0$ and the reverse trend when $K=1$. This is because for the case $K=0$, the Lorentz force is acting perpendicularly to direction of flow formation and therefore slowing down fluid velocity. Conversely, the

Lorentz force when $K = 1$ is acting in such a way that it assist flow formation and therefore increasing velocity profile in the annulus.

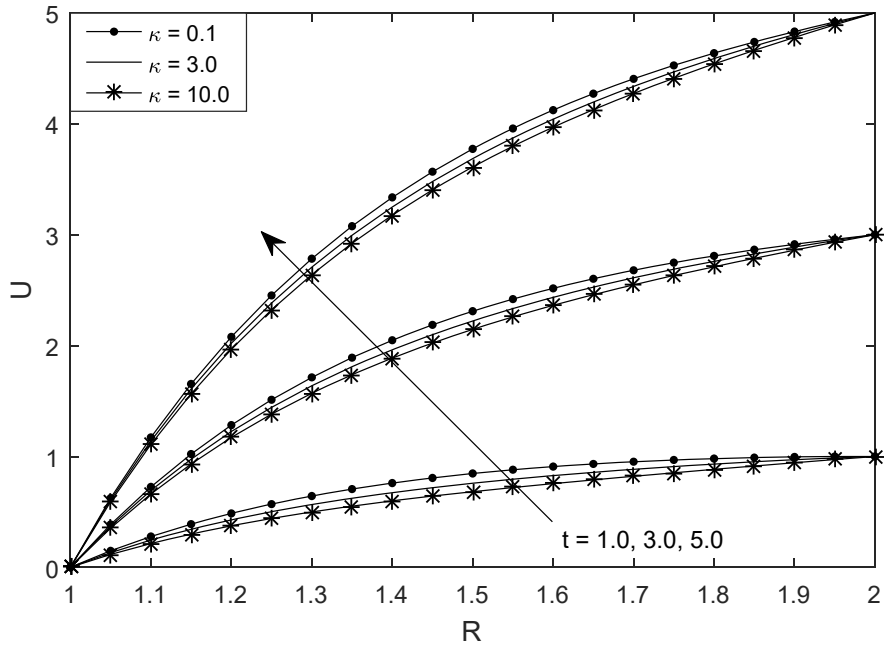

Fig.3b. Velocity profile for different values of κ at different time t for $M = 2.0$, $\lambda = 2.0$, $G = 2.0$, $\zeta_r = 1.0$, $K = 1$.

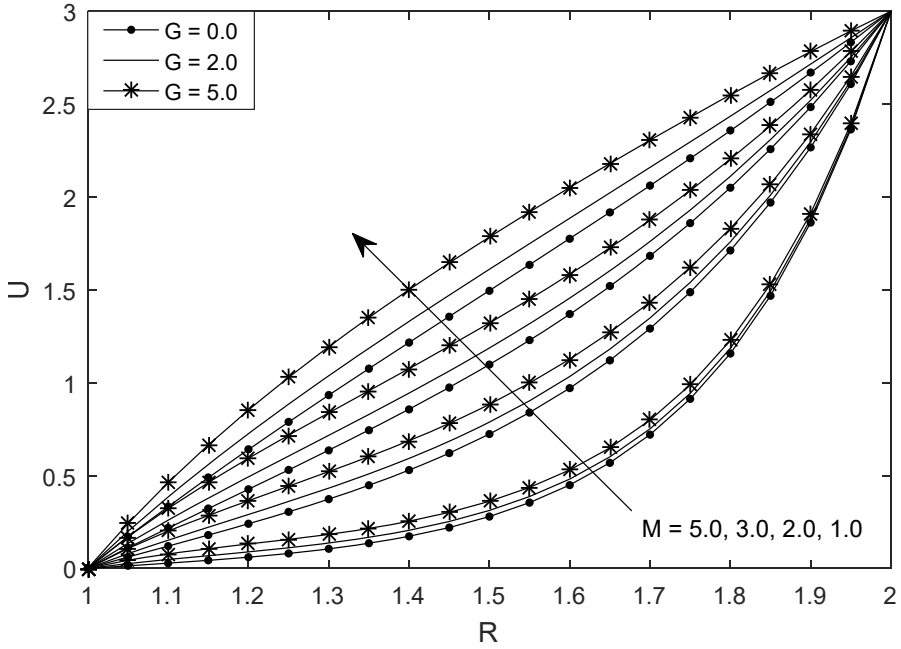

Fig.4a. Velocity profile for different values of G and M for $\kappa = 3.0$, $\lambda = 2.0$, $t = 3.0$, $\zeta_r = 1.0$, $K = 0$.

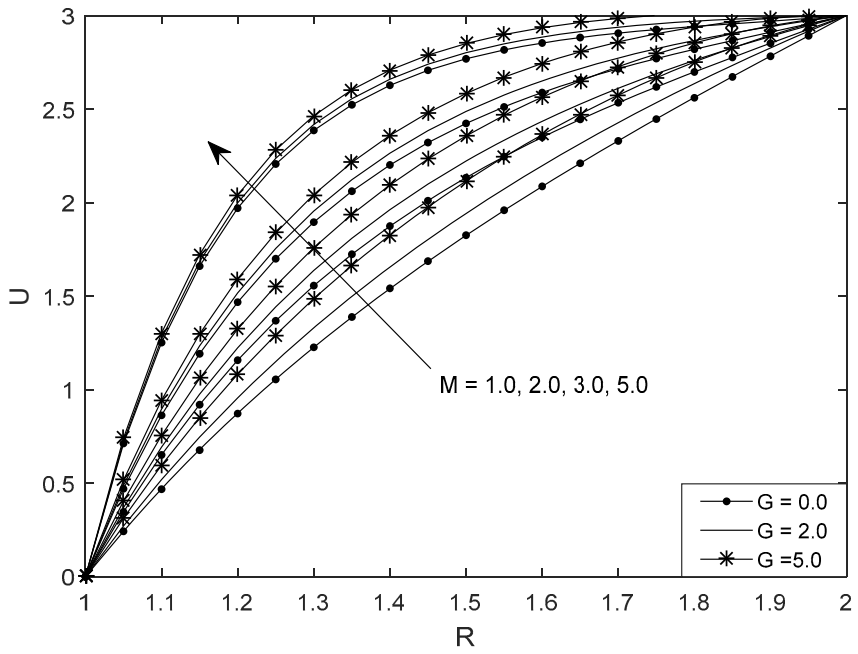

Fig.4b. Velocity profile for different values of G and M for $\kappa = 3.0$, $\lambda = 2.0$, $t = 3.0$, $\zeta_r = 1.0$, $K = 1$.

Skin-friction

This sub-section is dedicated to investigating the impact of electrokinetic effect and Hartmann number on time-dependent Couette flow in a horizontal annulus filled with electrically conducing fluid. The study of shear stress continues to gain significant attention due to its engineering and technological applications, such as; high speed jets, construction of bridges and dams.

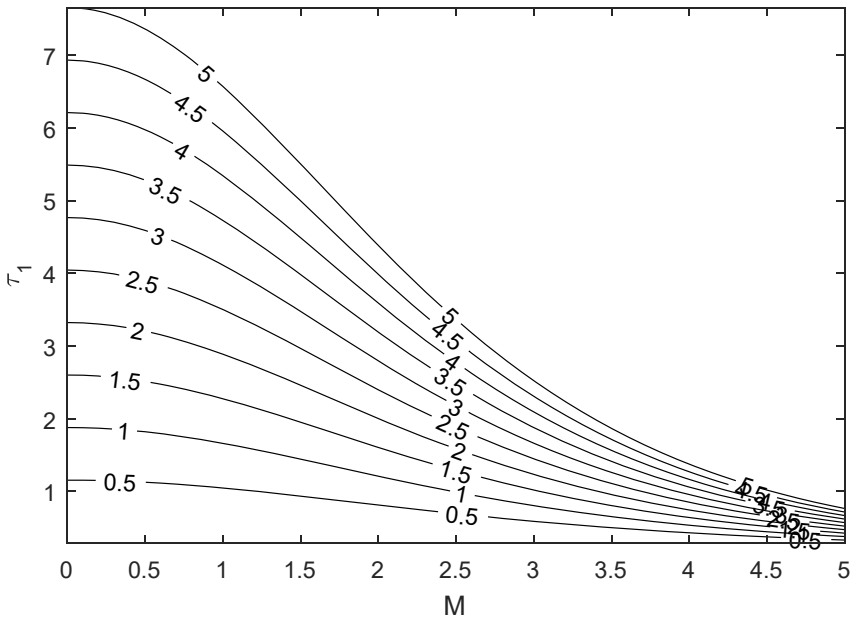

Fig.5a. Skin-friction at the outer surface of the inner cylinder for different values of t and M at $G = 2.0$, $\kappa = 3.0$, $\zeta_r = 1.0$, $K = 0$ $(R = 1.0)$.

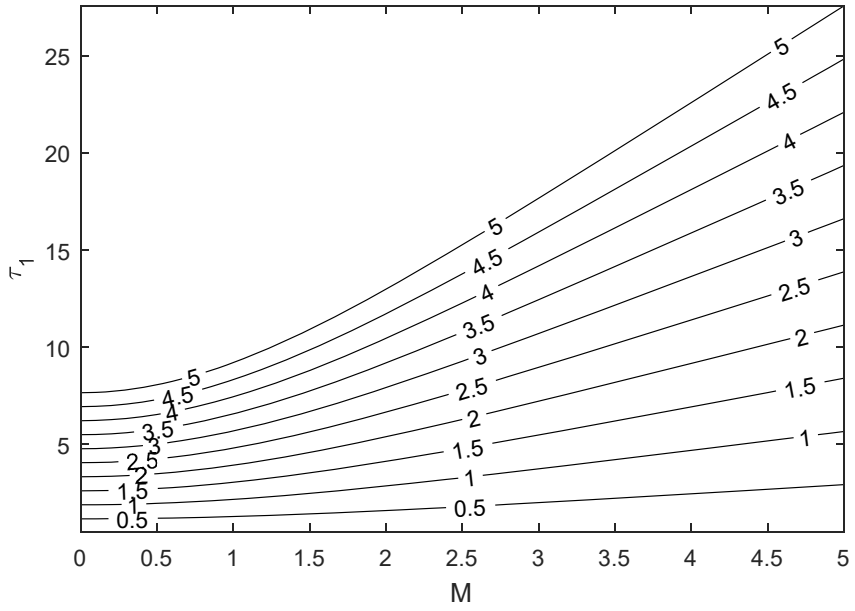

Fig.5b. Skin-friction at the outer surface of the inner cylinder for different values of *t* and *M* at $G = 2.0$, $\kappa = 3.0$, $\zeta_r = 1.0$, $K = 1\ (R = 1.0)$.

Figures 5a and 5b exhibit the joint role of magnetic field (M) and dimensionless time (t) on skin friction at the outer surface of inner cylinder for $K = 0$ and $K = 1$ respectively in the presence of EDL. Result indicates that skin-friction increases with time irrespective of the mode of application of magnetic field. On the other hand, skin-friction declines with surge in M when magnetic field is fixed relative to the fluid and increases otherwise. A careful look at Fig.5a advises that skin friction can be reduced to nothing in the presence of very strong magnetic field $(M \to \infty)$, whereas in Fig.5b, skin-friction can be reduced $M \to 0$ at the starting time of flow formation.

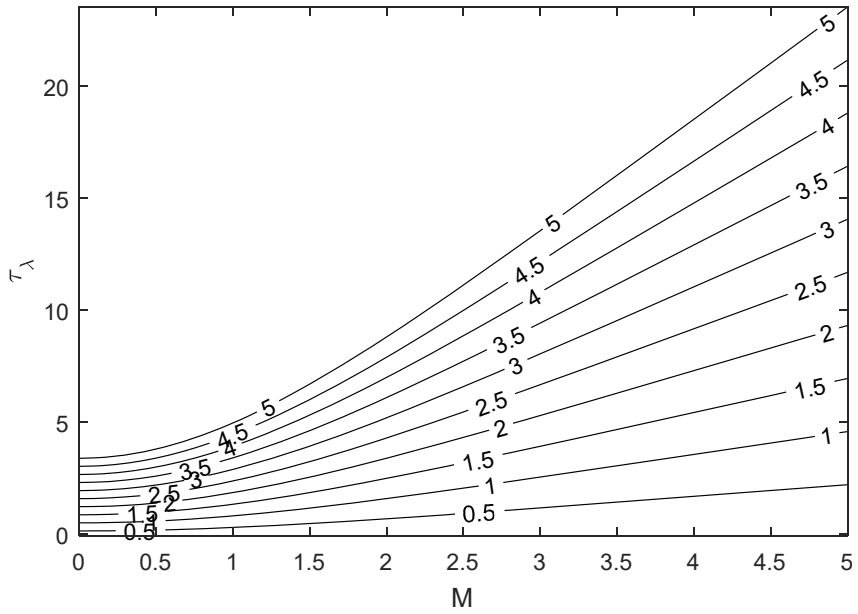

Fig.6a. Skin-friction at the inner surface of the outer cylinder for different values of *t* and *M* at $G = 2.0$, $\kappa = 3.0$, $\zeta_r = 1.0$, $K = 0\ (R = 2.0)$.

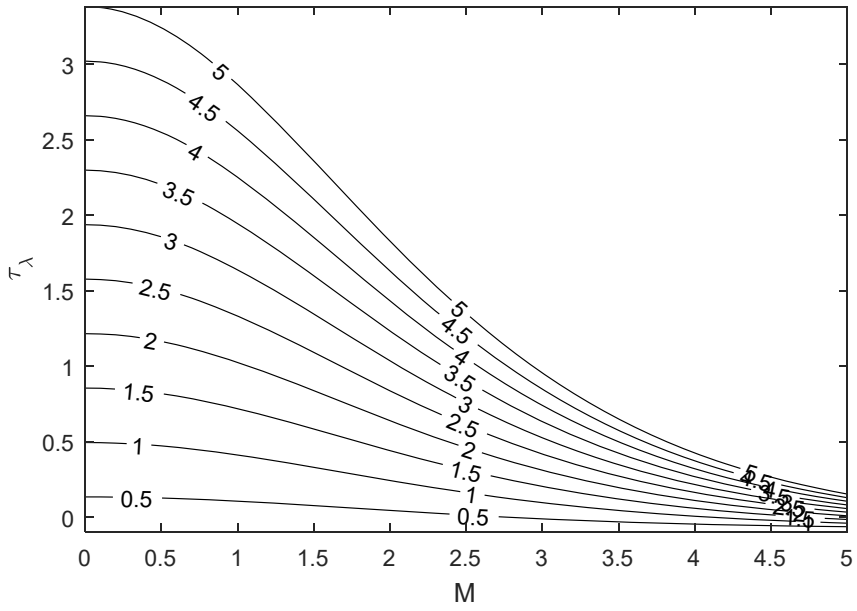

Fig.6b. Skin-friction at the inner surface of the outer cylinder for different values of t and M at $G = 2.0,\ \kappa = 3.0,$ $\zeta_r = 1.0,\ K = 1\ (R = 2.0)$.

Figures 6a and 6b show skin-friction at the inner surface of the outer cylinder for different values of M at different time for $K = 0$ and $K = 1$ respectively. The reverse trend of Figs. 5a and 5b is found in Figs 6a and 6b where skin-friction increases with M at $K = 0$ and decreases at $K = 1$. This difference in result is due to the direction of analysis, in fact, this can be tagged as another checkmate for accuracy test.

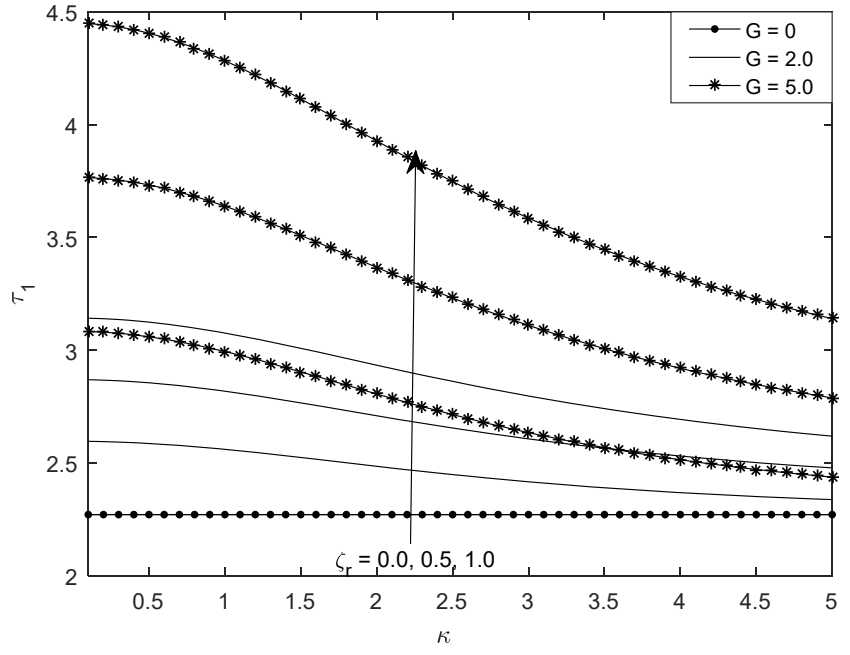

Fig.7a. Skin-friction at the outer surface of the inner cylinder for different values of κ, G and ζ_r at $M = 2.0,$ $t = 3.0,\ K = 0, \lambda = 2.0\ (R = 1.0)$.

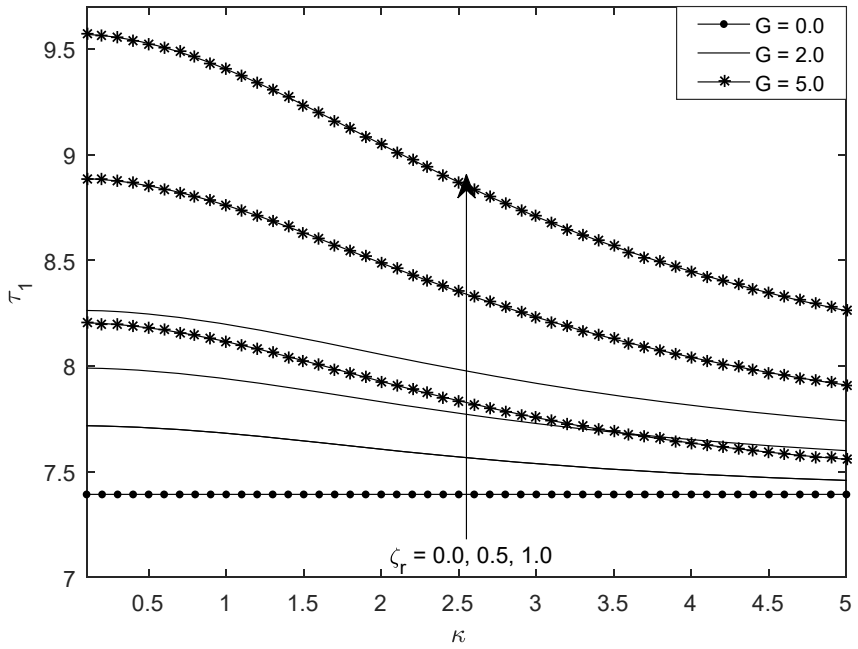

Fig.7b. Skin-friction at the outer surface of the inner cylinder for different values of κ, G and ζ_r at $M = 2.0$, $t = 3.0,\ K = 1, \lambda = 2.0\ (R = 1.0)$.

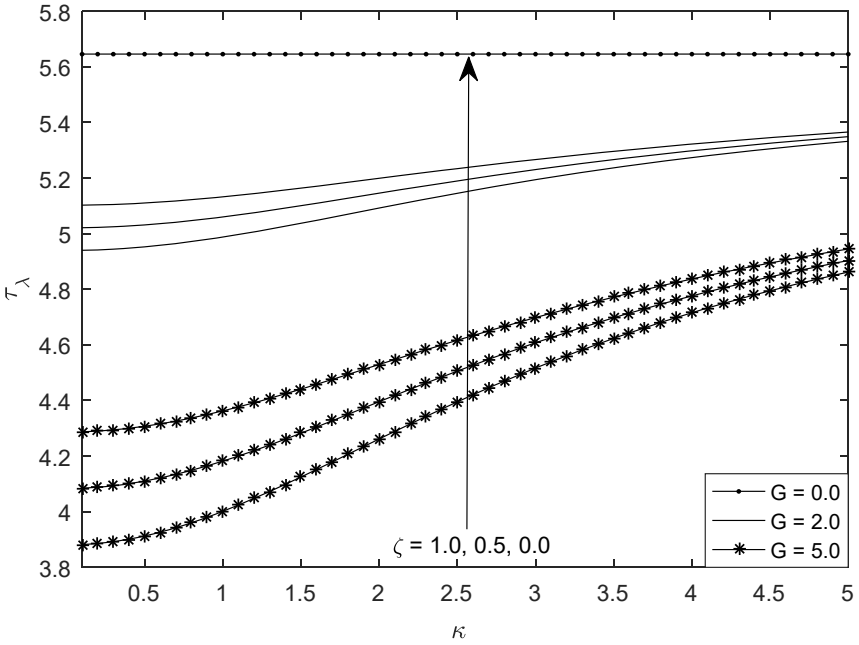

Fig.8a. Skin-friction at the inner surface of the outer cylinder for different values of κ, G and ζ_r at $M = 2.0$, $t = 3.0,\ K = 0, \lambda = 2.0\ (R = 2.0)$.

Figures 7a and 7b demonstrate the combined role of zeta potential (ζ_r) and magnitude of EDL (G) on skin friction at cylinder surface for the cases $K = 0$ and $K = 1$ respectively. From these figures, the impact of electrokinetic effect is to increase skin-friction at this surface of the cylinder regardless of the mode of application of magnetic field.

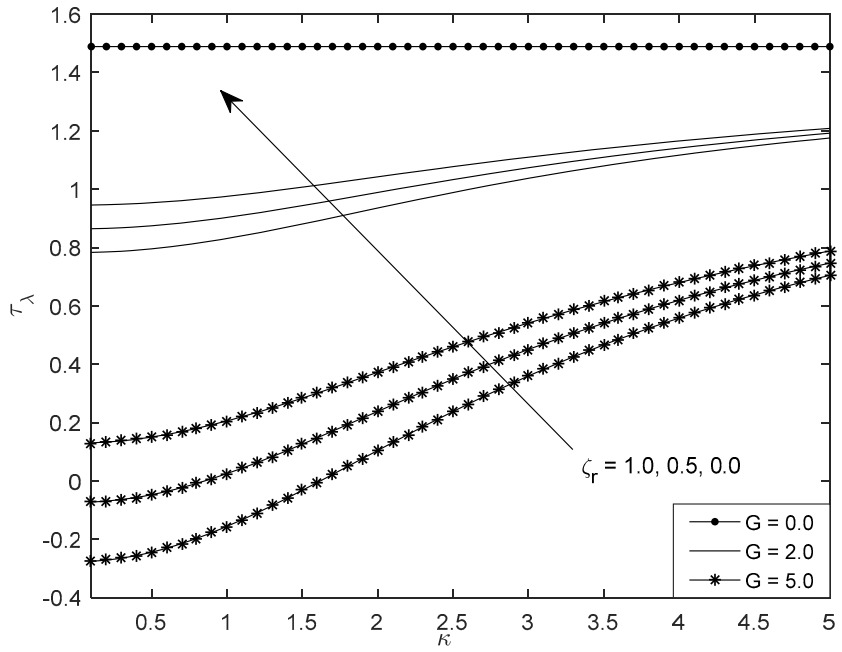

Fig.8b. Skin-friction at the inner surface of the outer cylinder for different values of κ, G and ζ_r at $M = 2.0$, $t = 3.0,\ K = 1.0, \lambda = 2.0\ (R = 2.0)$.

As check on accuracy, it is gotten that skin friction is not dependent of κ for $G = 0$. Another important note from this figure is that skin friction declines with rise in κ. This is expected because rise in κ signifies a thin EDL and therefore reducing the collisions in the horizontal annulus and hence reducing the force at which the electrically conducting fluid hits the outer surface of the inner cylinder. Further, $G = 0$ signifies that the only force responsibility for drag effect is due to the accelerated movement of the cylinder, therefore lower relative to the combined effect of electrokinetics in the horizontal annulus. A watchful look at these figures recommends that as $\kappa \to \infty$ (which corresponds to no EDL), electrokinetic effect plays no role in the overall skin friction at the outer surface of inner cylinder irrespective of its magnitude. The skin friction is established to be maximum on the outer surface of inner cylinder for the case of symmetric zeta potential and when $K = 1$. One can recommend that the accelerated motion of the inner surface of outer cylinder leads to a decline in skin-friction at this surface.

Figures 8a and 8b on the other hand present the skin friction at the inner surface of outer cylinder for $K = 0$ and $K = 1$ respectively. A reverse trend of Figs 7a and 7b is observed. This is expected since it is in opposite direction to the first analysis.

Mass flow-rate

Another distinctive analysis in the study of microfludic is the computation of the total fluid passing through the horizontal annulus in the fully developed state. Figures 9a and 9b portray the mass flowrate for diverse values of M at different time in the horizontal annulus for the cases when $K = 0$ and $K = 1$ respectively. It is observed that the amount of fluid continues to increase with time. This may be attributed to the continuous acceleration of the inner surface of the outer cylinder. Then again, the mass flow rate is observed to be a decreasing function of Hartmann number (M) when $K = 0$ and a converse result when $K = 1$. It is easy to conclude that for $K = 0$ in the presence of strong magnetic field $(M \to \infty)$, there may be stoppage of flow formation. This can be attributed to the Lorentz force acting perpendicularly to flow direction which would have been strong enough to stop flow formation as well as mass flow rate.

Figure 10 displays the effect of degree of electrokinetics and κ on mass flowrate in the horizontal annulus for the case of symmetric zeta potential. It is obtained that mass flowrate decreases with κ regardless of the mode of application of magnetic field. In addition, there exists a corresponding increase in Q with increase in G. As $\kappa \to \infty$, electrokinetic influence plays no role in the overall mass flow-rate regardless of the magnitude of the EDL, thereby corresponding to the results of absence of externally applied voltage $(G = 0)$.

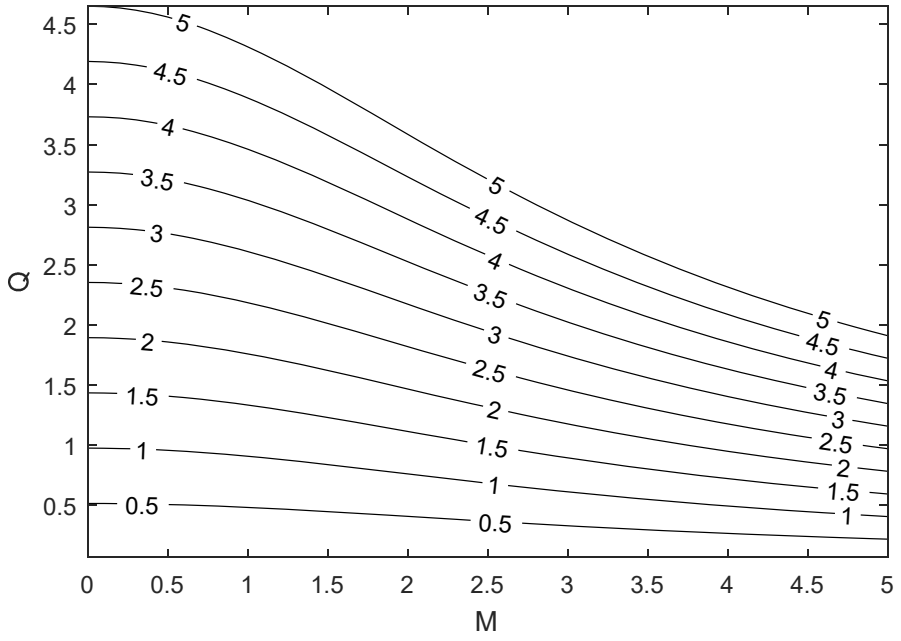

Fig.9a. Mass flow-rate for different values of *M* and *t* at $\lambda = 2.0,\ \kappa = 3.0,\ G = 2.0,\ K = 0,\ \zeta_r = 1.0$.

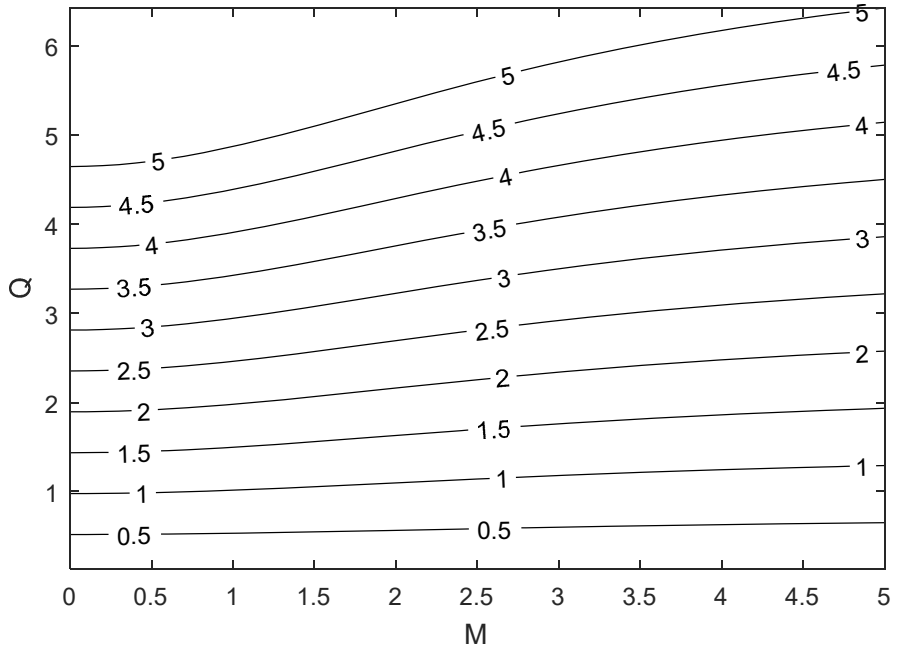

Fig.9b. Mass flow-rate for different values of *M* and *t* at $\lambda = 2.0,\ \kappa = 3.0,\ G = 2.0,\ K = 1,\ \zeta_r = 1.0$.

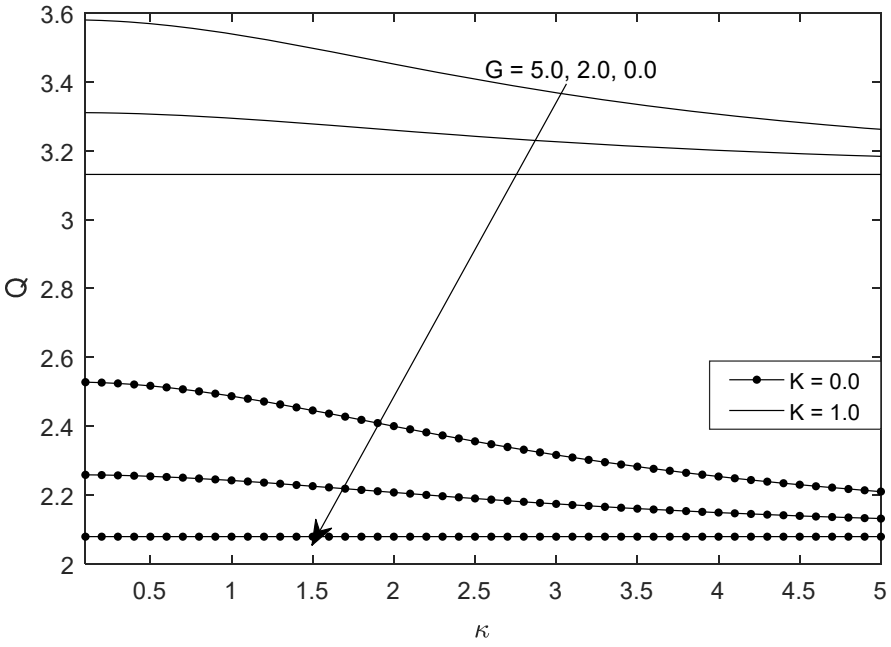

Fig.10. Mass flow-rate for different values of κ, G and K at $t = 3.0$, $\zeta_r = 1.0$, $M = 2.0$, $\lambda = 2.0$.

4. Conclusion

The time-dependent Couette flow of a conducting fluid in a horizontal annulus with combined role of electrokinetic and accelerated motion of outer cylinder is considered in this article. The governing equations are presented and changed to their various dimensionless forms by means of fit dimensionless parameters. Using Laplace transform technique, analytical solutions for electric field and fluid velocity are obtained. Based on the graphical represented of the obtained solutions, the subsequent inferences are drawn:

1. Velocity, mass flowrate and skin-friction decrease with increase in Debye-Hückel parameter at all-time regardless of the mode of application of magnetic field.
2. Rise in the magnitude of electrokinetic results to corresponding rise in fluid velocity, mass flowrate and skin-friction.
3. Mass flow-rate is enhanced when magnetic field is fixed relative to the moving cylinder than when it is fixed relative to the fluid.
4. The combined presence of strong magnetic field and Debye-Hückel parameter can lead to no flow and consequently zero skin-friction at the outer surface of inner cylinder.
5. Magnetic field and accelerated motion of the outer cylinder can serve as control mechanisms to lower or enhance the mass flow rate.

Nomenclature

c_0 – concentration of ions in bulk fluid

B – magnetic field induction vector

B_0 – magnetic field strength

$E_{z'}$ – electrostatic intensity

F – Faraday's constant

g – acceleration due to gravity

G – dimensionless parameter

J – current density vector
M – Hartmann number
m' – positive integer
LT – Laplace transform
R – dimensionless radial coordinate
R' – universal gas constant
r – dimensional radial coordinate
r_1 – radius of inner cylinder
r_2 – radius of outer cylinder
T – temperature of the fluid
t – dimensionless time
U – dimensionless velocity
u – dimensional velocity
u' – constant reference velocity
$\bar{v}$ – vectorial velocity profile
z – valence number of ions in the solution
z' – axial coordinate
ε – fluid permittivity
ζ – zeta – potential (electrokinetic potential of the wall in the double layer)
ζ_r – ζ_2/ζ_1 (dimensionless)
η – dimensional time
κ – Debye-Huckel parameter
λ – annular gap $\left(\lambda = \frac{r_2}{r_1}\right)$
λ_D – Debye length
μ – fluid dynamic viscosity
ν – kinematic viscosity
ρ – fluid density
ρ_f – fluid density
ρ_e – charge density
σ – electrical conductivity of the fluid
τ – skin-friction
Φ – externally imposed electrostatic potential
ϕ – electrostatic potential
ψ – dimensionless EDL potential
ψ' – dimensional EDL potential

Subscripts

1 – value at the surface $r = r_1$
λ – value at the surface $r = r_2$

References

[1] Wall S. (2010): *The history of electrokinetic phenomena*.– Current Opinion in Colloid & Interface Science, vol.15, No.3, pp.119-124.

[2] Karniadakis G., Beskok A. and Aluru N. (2005): *Microflows and Nanoflows: Fundamentals and Simulation*.– Springer, New York, pp.231.

[3] Chang L., Jian Y., Buren M., Liu Q. and Sun Y. (2016): *Electroosmotic flow through a microtube with sinusoidal roughness*.– Journal of Molecular Liquids, vol.220, pp.258-264.

[4] Rojas G., Arcos J., Peralta M., Méndez F. and Bautista O. (2017): *Pulsatile electroosmotic flow in a microcapillary with the slip boundary condition*.– Colloids and Surfaces A: Physicochemical and Engineering Aspects, vol.513, pp.57-65.

[5] Probstein R.F. (2005): *Physicochemical Hydrodynamics: An Introduction*.– John Wiley & Sons, pp.342.

[6] Laser D.J. and Santiago J.G. (2004): *A review of micropumps*.– Journal of Micromechanics and Microengineering, vol.14, No.6, pp.35.

[7] Chakraborty J., Ray S. and Chakraborty S. (2012): *Role of streaming potential on pulsating mass flow rate control in combined electroosmotic and pressure-driven microfluidic devices*.– Electrophoresis vol.33, pp.419-425.

[8] Chakraborty S. and Ray S. (2008): *Mass flow-rate control through time periodic electro-osmotic flows in circular microchannels*.– Physics of Fluids, vol.20, No.8, pp.1-11.

[9] Kirby B.J. and Hasselbrink Jr E.F. (2004): *Zeta potential of microfluidic substrates: 2. Data for polymers*.– Electrophoresis, vol.25, No.2, pp.203-213.

[10] Wang C.Y., Liu Y.H. and Chang C.C. (2008): *Analytical solution of electro-osmotic flow in a semicircular microchannel*.– Physics of Fluids, vol.20, No.6, pp.1-6.

[11] Jian Y., Yang L. and Liu Q. (2010): *Time periodic electro-osmotic flow through a microannulus*.– Physics of Fluids, vol.22, No.4, pp.1-7.

[12] Khaki M., Taeibi-Rahni M. and Ganji D.D. (2012): *Analytical solution of electro-osmotic flow in rectangular nano-channels by combined sine transform and MHPM*.– Journal of Electrostatics, vol.70, No.5, pp.451-456.

[13] Arulanandam S. and Li D. (2000): *Liquid transport in rectangular microchannels by electroosmotic pumping*.– Colloids and Surfaces A: Physicochemical and Engineering Aspects, vol.161, No.1, pp.89-102.

[14] Katagiri M. (1962): *Flow formation in Couette motion in magnetohydrodynamics*.– Journal of the Physical Society of Japan, vol.17, No.2, pp.393-396.

[15] Muhuri P. (1963): *Flow formation in Couette motion in magnetohydrodynamics with suction*.– Journal of the Physical Society of Japan, vol.18, No.11, pp.1671-1675.

[16] Singh A.K. and Kumar N. (1983): *Unsteady magnetohydrodynamic Couette flow*.– Wear, vol.89, No.2, pp.125-129.

[17] Globe S. (1959): *Laminar steady-state magnetohydrodynamic flow in an annular channel*.– The Physics of Fluids, vol.2, No.4, pp.404-407.

[18] Jha B.K. and Oni M.O. (2018): *Impact of mode of application of magnetic field on rate of heat transfer of rarefied gas flows in a microtube*.– Alexandria Engineering Journal, vol.57, No.3, pp.1955-1962.

[19] Jha B.K., Aina B. and Isa S. (2015): *Fully developed MHD natural convection flow in a vertical annular microchannel: an exact solution*.– Journal of King Saud University-Science, vol.27, No.3, pp.253-259.

[20] Jha B.K. and Aina B. (2016): *Role of induced magnetic field on MHD natural convection flow in vertical microchannel formed by two electrically non-conducting infinite vertical parallel plates*.– Alexandria Engineering Journal, vol.55, No.3, pp.2087-2097.

[21] Jha B.K. and Oni M.O. (2018): *Fully developed mixed convection flow in a vertical channel with electrokinetic effects: exact solution*.– Multidiscipline Modeling in Materials and Structures, vol.14, No.5, pp.1031-1041.

[22] Jha B.K. and A. Apere C. (2010): *Unsteady MHD Couette flows in an annuli: the Riemann-sum approximation approach*.– Journal of the Physical Society of Japan, vol.79, No.12, pp.1244-1247.

[23] Oni M.O. and Jha B.K. (2023): *Entropy generation analysis of electroosmotic mixed convection flow in vertical microannulus with asymmetric heat fluxes*.– Int. Commun. Heat Mass Transf., vol.145, pp.1068-1081.

[24] Oni M.O. and Rilwan U. (2023): *Role of suction/injection on electromagnetohydrodynamic natural convection flow in a porous microchannel with electroosmotic effect*.– Int. J. of Applied Mechanics and Engineering, vol.28, No.4, pp.94-113.

[25] Oni M.O. and Jha B.K. (2022): *Analysis of transient buoyancy/electroosmotic driven flow in a vertical microannulus*

with velocity-slip and temperature-jump.– Eng. Sci. Technol., pp.84-107, https://doi.org/10.37256/est.3120221293.

[26] Oni M.O., Rilwan U., Jha B.K. and Jibril H.M. (2023): *Analysis of Joule heating and viscous dissipation on electromagnetohydrodynamic flow with electroosmotic effect in a porous microchannel: A heat transfer miniature enhancement*.– Heat Transf. (in press), DOI: 10.1002/htj.22974.

[27] Khadrawi A.F. and Al-Nimr M.A. (2007): *Unsteady natural convection fluid flow in a vertical microchannel under the effect of the dual-phase-lag heat-conduction model.*– International Journal of Thermophysics, vol.28, pp.1387-1400.

[28] Tzou D.Y. (2014): *Macro -to Microscale Heat Transfer: The Lagging Behavior*.– John Wiley & Sons, DOI:10.1002/9781118818275.

[29] Jha B.K. and Oni M.O. (2018): *Transient natural convection flow between vertical concentric cylinders heated/cooled asymmetrically*.– Proceedings of the Institution of Mechanical Engineers, Part A: Journal of Power and Energy, vol.232, No.7, pp.926-939.

[30] Mukhopadhyay A., Banerjee S. and Gupta C. (2009): *Fully developed hydrodynamic and thermal transport in combined pressure and electrokinetically driven flow in a microchannel with asymmetric boundary conditions*.– International Journal of Heat and Mass Transfer, vol.52, No.8, pp.2145-2154.

Received: February 1, 2024
Revised: June 24, 2024